THE JOURNAL OF PHYSICAL CHEMISTRY B

Article

pubs.acs.org/JPCB

# Experimental and Theoretical Study on the One- and Two-Photon Absorption Properties of Novel Organic Molecules Based on Phenylacetylene and Azoaromatic Moieties

Marcelo G. Vivas,*[,†] Daniel L. Silva,[‡] Leonardo De Boni,[†] Yann Bretonniere,[§] Chantal Andraud,[§] Florence Laibe-Darbour,[∥] J.-C. Mulatier,[∥] Robert Zaleśny,[⊥] Wojciech Bartkowiak,[⊥] Sylvio Canuto,[‡] and Cleber R. Mendonca*[,†]

[†]Instituto de Física de São Carlos, Universidade de São Paulo, Caixa Postal 369, 13560-970 São Carlos, SP, Brazil

[‡]Instituto de Física, Universidade de São Paulo, CP 66318, 05314-970, São Paulo, SP, Brazil

[§]CNRS, Université Lyon I, ENS-Lyon, 46 alléed'Itale, 69364 Lyon, France

[∥]Laboratoire de Chimie, CNRS UR 5182, ENS de Lyon, Université Lyon I, 46 alléed'Italie, 69364 Lyon cedex 07, France

[⊥]Theoretical Chemistry Group, Institute of Physical and Theoretical Chemistry, Wroclaw University of Technology, WybrzezeWyspianskiego 27, 50-370 Wroclaw, Poland

Supporting Information

**ABSTRACT:** This Article reports a combined experimental and theoretical analysis on the one and two-photon absorption properties of a novel class of organic molecules with a $\pi$-conjugated backbone based on phenylacetylene (**JCM874**, **FD43**, and **FD48**) and azoaromatic (**YB3p25**) moieties. Linear optical properties show that the phenylacetylene-based compounds exhibit strong molar absorptivity in the UV and high fluorescence quantum yield with lifetimes of approximately 2.0 ns, while the azoaromatic-compound has a strong absorption in the visible region with very low fluorescence quantum yield. The two-photon absorption was investigated employing nonlinear optical techniques and quantum chemical calculations based on the response functions formalism within the density functional theory framework. The experimental data revealed well-defined 2PA spectra with reasonable cross-section values in the visible and IR. Along the nonlinear spectra we observed two 2PA allowed bands, as well as the resonance enhancement effect due to the presence of one intermediate one-photon allowed state. Quantum chemical calculations revealed that the 2PA allowed bands correspond to transitions to states that are also one-photon allowed, indicating the relaxation of the electric-dipole selection rules. Moreover, using the theoretical results, we were able to interpret the experimental trends of the 2PA spectra. Finally, using a few-energy-level diagram, within the sum-over-essential states approach, we observed strong qualitative and quantitative correlation between experimental and theoretical results.

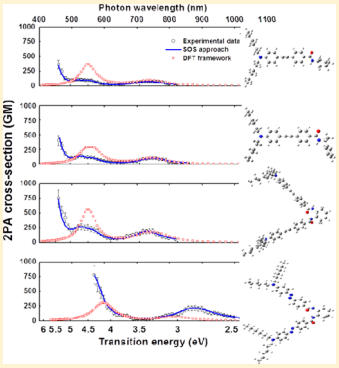


## I. INTRODUCTION

The study of photochemical properties of new two-photon absorbing materials has increased considerably in the past years because of their remarkable features for various applications such as three-dimensional (3D) optical data storage,[1] fluorescence imaging,[2] photodynamic therapy,[3] frequency upconverted lasing,[4] optical limiting,[5] coherent control,[6] microfabrication and micromachining,[7,8] and so on. Such applications are basically associated with two intrinsic characteristics of two-photon absorption (2PA): (i) excitation takes place in the near-IR spectral region where damage and scattering are smaller than in the UV−visible and (ii) the quadratic dependence on intensity, which allows high spatial localization of the excitation. These characteristics allow developing photonic devices from optics to biology.

Among the different types of materials used for such purposes, organic compounds provide advantages in relation to others, since their optical properties can be easily modified or optimized by molecular engineering strategies. For this reason, great efforts have been aimed at this type of chromophores to increase and tune 2PA properties. Depending on the applications, two-photon absorbing chromophores have to satisfy different requirements. For example, combination of high fluorescence quantum yield and 2PA cross-section in the red−near-infrared (NIR) range are desirable for biological imaging;[2,9] while very high 2PA cross-section (>$10^3$ GM) and chemical reactions are necessary for 3D optical data storage.[10] However, a great number of factors influence the 2PA properties: electronic delocalization,[11] degree of molecular planarity,[12,13] intramolecular charge transfer,[14] bond length alternation,[15,16] cooperative enhancement between branches,[17] temperature effect,[18,19] and so on. Therefore, to explore the full potential of a material envisioning applications, it is necessary

**Received:** October 30, 2012
**Published:** November 21, 2012

**Chart 1. Structures of the Push−Pull Dipolar Molecules Studied Based on Phenylacetylene (JCM874, FD43, and FD48) and Azoaromatic (YB3p25) Moieties**

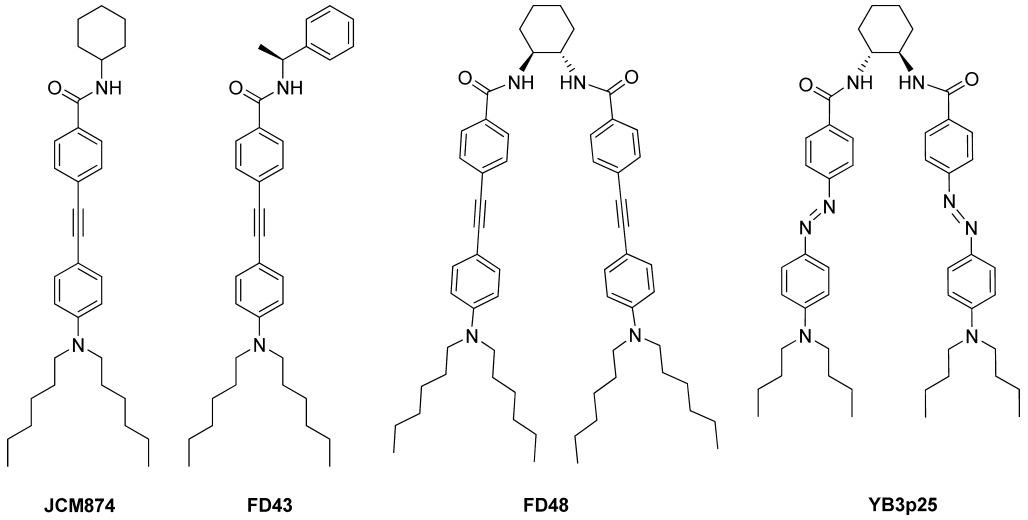


**Scheme 1. Preparation of the Azo (YB3p25) and Phenylacetylene Compounds (JCM874, FD43, and FD48)[a]**

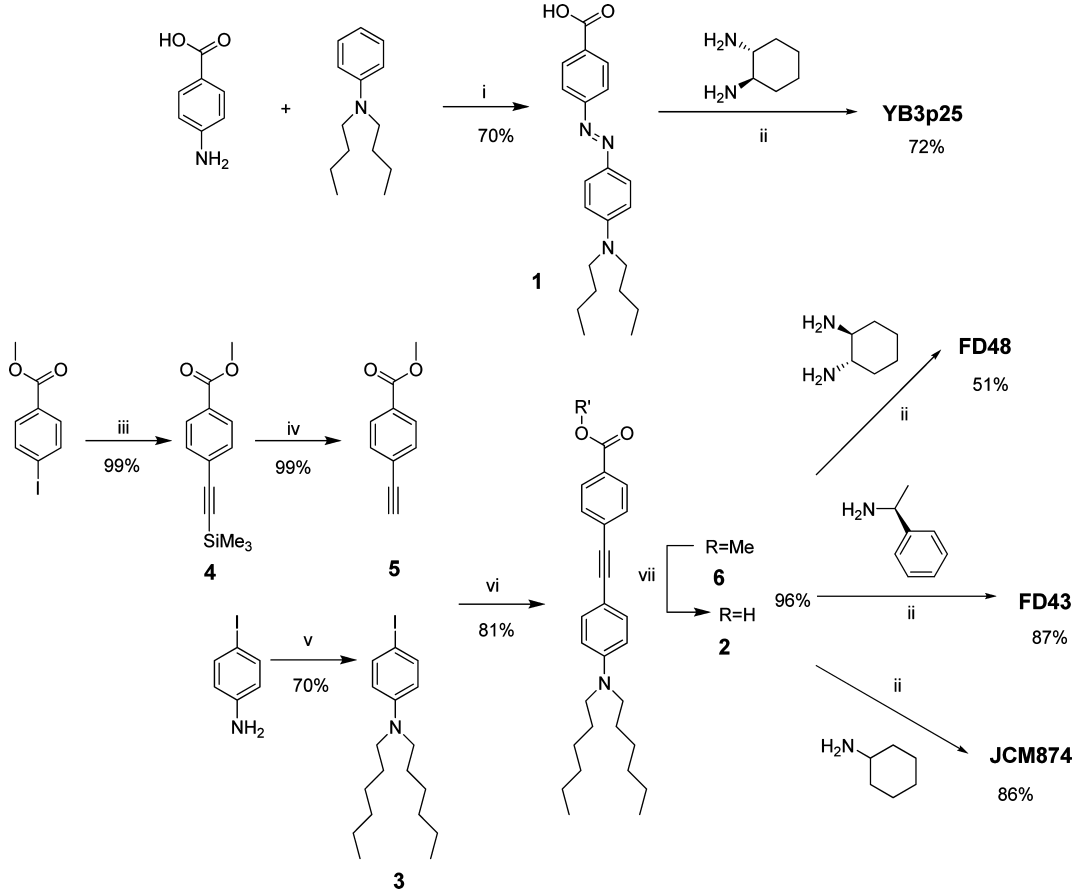


[a]Reagents and conditions: (i) $NaNO_2$, HCl, $H_2O$, 0 °C, 0.5 h then NaOAc, 0 °C, 0.5 h; (ii) DIC, HOBt, $CH_2Cl_2$, DMF, r.t., 15 h; (iii) ethynyltrimethylsilane, $PdCl_2(PPh_3)_2$, CuI, THF, $Et_3N$, 80 °C, 2 h, or r.t., 15 h; (iv) $K_2CO_3$, MeOH, 0.5 to 3 h; (v) *N*,*N*-dihexyl-4-iodobenzenamine, $PdCl_2(PPh_3)_2$, CuI, THF, $Et_3N$, r.t., 24 h; (vi) 1-bromohexane, NaI, $Na_2CO_3$, DMF, 100 °C, 48 h; (vii) methyl 4-iodobenzoate, $PdCl_2(PPh_3)_2$, CuI, THF, $Et_3N$, r.t., 15 h; (viii) LiOH, n-$Bu_4NOH$, MeOH, r.t., 72 h.

to investigate the relationship between chemical structure and optical properties. In particular, structures containing $\pi$-conjugated bridges based on phenylacetylene and azoaromatic moieties, with asymmetrical D-$\pi$-A or symmetrical D-$\pi$-A-$\pi$-D structures (D = donor group; $\pi$ = conjugated; A = acceptor group), have led to a large charge redistribution of chromophore upon excitation, increasing the dipole moment and consequently the 2PA cross-section.[20−22] In this context,


dx.doi.org/10.1021/jp310731t | J. Phys. Chem. B 2012, 116, 14677−14688

we synthesized and studied a novel class of organic materials containing $\pi$-conjugated backbone based on phenylacetylene (**JCM874**, **FD43**, and **FD48**) and azoaromatic (**YB3p25**) moieties (Chart 1). As can be observed in Chart 1, **FD43** presents molecular chirality because of the chiral carbon attached to the phenyl ligand, while the chirality of **FD48** and **YB3p25** is due to their helical molecular structure. Such designs are interesting in organic chemistry because they allow structural improvements of organic compounds to study light-matter interactions beyond the electric dipole approximation as, for instance, electric quadrupole and magnetic dipole interactions.

To investigate the broadband one- and two-photon optical properties of this class of organic materials, we used the wavelength-tunable femtosecond Z-scan technique and quantum chemical calculations. The nonlinear spectra were modeled using the sum-over-essential states approach, which was supported by theoretical predictions of the two-photon transitions strengths carried out using the response functions formalism within the density functional theory (DFT) framework.[23] Recently, the 2PA spectroscopy in conjunction with quantum chemical calculations have proven to be a powerful tool to determine molecular parameters of organic molecules, such as "dark" states, transition dipole moments and permanent dipole moment changes, and so on.[24−26] To check for saturation and/or photodegradation processes during the measurements, we measured the fluorescence intensity and normalized transmittance, excited via femtosecond pulses, as a function of irradiance. Linear optical properties such as molar absorptivity, one-photon-induced fluorescence, fluorescence quantum yield, and lifetimes are also reported.

## II. EXPERIMENTAL SECTION

The amides **YB3p25**, **JCM874**, **FD43**, and **FD48** were synthesized from the carboxylic acids **1**[27] and **2** and the corresponding amine using diisopropylcarbodiimide and *N*-hydroxybenzotriazole as coupling agents (see Scheme 1). *N*-hydroxybenzotriazole was preferred to the more commonly used 4-dimethylaminopyridine as it was found to give much better yield and less side products. The carboxylic acid **2** was obtained in five steps and very good yield from *N*,*N*-dihexyl-4-iodobenzenamine (**3**) and methyl 4-iodobenzoate by a double Sonogashira coupling giving the ester **6**, followed by saponication of the ester. Details about the synthesis can be found in the Supporting Information.

Solutions of the organic molecules in chloroform were prepared, with concentrations around $1 \times 10^{-4}$ and $5 \times 10^{-3}$ mol $L^{-1}$ for linear and nonlinear optical measurements, respectively. The samples were placed in 2 mm thick quartz cuvettes for optical measurements. The linear absorption and photoluminescence (PL) spectra were recorded using a standard spectrophotometer and fluorimeter, respectively. Nonlinear optical measurements were carried out employing the open aperture Z-scan technique, using 120-fs laser pulses from an optical parametric amplifier pumped by 150-fs pulses (775 nm) from a Ti:sapphire chirped pulse amplified system, operating at 1-kHz repetition rate. The Z-scan measurements were carried out with intensities ranging from 30 to 200 GW/cm$^2$ (10 to 130 nJ/pulse) and with beam waist size from 14 to 21 $\mu$m. The same laser system was used to excite the samples fluorescence, which was collected perpendicularly to excitation through an optical fiber attached to a spectrometer. The fluorescence intensity was measured as a function of the excitation irradiance at the peak of the lowest energy 2PA band appearing along the nonlinear spectrum.

For an absorptive nonlinearity, the light field induces an intensity dependent absorption coefficient, $\alpha = \alpha_0 + \beta I$, where $I$ is the laser beam intensity, $\alpha_0$ is the linear absorption coefficient, and $\beta$ is the 2PA coefficients. After carrying out the open aperture measurement, the nonlinear absorption coefficient can be unambiguously determined by fitting the experimental data. The 2PA cross-section can be obtained through the expression $\sigma_{2PA} = \hbar\omega\beta/N$, where $N$ is the number of molecules per cubic centimeter (cm$^3$), and $\hbar\omega$ is the photon energy.

To measure the fluorescence lifetime of the samples, pulses at 266 nm generated by doubling the second harmonic of a Q-switched and mode-locked Nd:YAG (70 ps). The 266 nm beam was focused into the sample, placed in a 2 mm-thick fused silica cuvette, with a lens of focal length $f$ = 12 cm. Experimental details about the time-resolved fluorescence setup can be found in ref 28.

To model the fluorescence lifetime, we used the deconvolution method. In this approach the deconvoluted fluorescence signal, $S(t)$, is given by

$$S(t) = \int G(t - t')I(t')\,dt' \tag{1}$$

where $I(t')$ is the system response function to the laser pulse, and $G(t)$ is the function that describes the fluorescence decay. Herein, we assume the system response function as a Gaussian ($I(t')$) with temporal full width at half-maximum (FWHM) of approximately 0.5 ns, because of the response time of silicon photodetector used, and a monoexponential function to describe the fluorescence behavior ($G(t)$).

To support our interpretation of the results, we estimated the expected fluorescence lifetime using the Strickler−Berg (SB) equation,[29,30] which related the molar absorptivity of the lowest energy absorption band and the fluorescence peak with the radiative lifetime, $\tau_0^{SB}$, as follows:

$$(\tau_0^{SB})^{-1} = \frac{1}{N_A} 8\pi n^2 c[2303(\upsilon_{em}^{max})^3] \int \frac{\varepsilon(\upsilon_A)}{\upsilon_A}\,d\upsilon_A \tag{2}$$

where $\upsilon_{em}^{max}$ and $\upsilon_A$ are the maximum emission and absorption wavenumber, respectively. To obtain the fluorescence lifetime, $\tau_f^{SB}$, it is necessary to calculate the product between the radiative lifetime given by eq 2 and the experimental fluorescence quantum yield, $\phi$.

## III. COMPUTATIONAL DETAILS

Due to the size of the studied molecules, all quantum-chemical calculations were performed using the Kohn−Sham formulation of density functional theory (KS-DFT). The equilibrium molecular geometries of the studied molecules were determined performing DFT calculations employing the hybrid exchange-correlation B3LYP[31,32] functional and the standard 6-311G(d,p) basis set[33] as implemented in the Gaussian 03 package.[34] Subsequently, to determine the lowest one- and two-photon allowed states of the studied molecules, the response functions calculations within the DFT framework were performed using the DALTON program.[35] In this approach, the excitation energies and transition dipole moments (two-photon probabilities) are analytically computed as poles and single residues of the linear (quadratic) response function of the molecular electronic density, respectively. Moreover, the

excited states dipole moments were also determined in the present work by computing the double residue of the quadratic response function. All the response function calculations were performed employing the hybrid exchange-correlation B3LYP[31,32] functional in combination with the standard 6-31+G(d) basis set[33] for molecules in vacuo. The 20 lowest energy transitions of each molecule were determined.

In this Article, using the two-photon transition probabilities and transition energies provided by quadratic response calculations, theoretical values were estimated for the 2PA cross-section and compared with the experimental data. The mathematical expression and a detailed description of the physical constants and photophysical parameters used to theoretically estimate the 2PA cross-section of a given excited state can be found in ref 36. The 2PA cross-section corresponding to the transition to a given excited state is inversely proportional to its spectral line width. It is important to mention that the line width of excited states vary, both from one molecule to another, as well as for different excited states within one molecule. Therefore, herein the excited state line widths of the molecules were estimated by fitting the experimental nonlinear spectra using a set of Lorentzian functions. The number of functions used in each fitting was defined based on the results of the quadratic response function calculations, which showed the number of 2PA allowed electronic states playing along the spectral region investigated for each molecule. Finally, a convolution of such Lorentzian functions, where the amplitude value adopted for each function was theoretically estimated from the 2PA cross-section of the respective excited state, was performed in order to simulate the 2PA cross-section spectrum of each compound. The simulated 2PA cross-section spectra are compared with the experimental nonlinear spectra.

## IV. RESULTS AND DISCUSSION

The molar absorptivity (solid lines) and fluorescence (empty squares) spectra of the **JCM874**, **FD43**, **FD48**, and **YB3p25** molecules are illustrated in Figure 1. Such spectra present a lowest energy absorption band between 320 and 420 nm for phenylacetylene (**JCM874**, **FD43**, and **FD48**) and 360−550 for azoaromatic derivatives with molar absorptivity magnitudes on the order of $3.5 \times 10^4$ mol$^{-1}$ L cm$^{-1}$ for **JCM874** and **FD43** and $6.5 \times 10^4$ mol$^{-1}$ L cm$^{-1}$ for **FD48** and **YB3p25**. Such transitions, in all molecules, are associated with the $\pi \rightarrow \pi^*$ transition from the $\pi$-conjugated backbone, while the higher energy bands are related to the electron donor and acceptor groups. As can be seen, **YB3p25** presents a significant bathochromic shift in the absorption (about 75 nm or 0.55 eV) with respect to molecules with $\pi$-conjugated bridge based on phenylacetylene due to the presence of the azo-group (−N═N−). Table 1 presents the photophysical parameters of the molecules studied here.

In Figure 1, the squares represent the PL spectra excited at the maximum of the linear absorption of each compound. Such spectra present a strong emission band centered at ca. 460 nm for phenylacetylene-based molecules. We did not measure the PL spectra for **YB3p25** because its fluorescence quantum yield is very small. It is known that a azoaromatic derivative presents weak radiative emission since most of its relaxation is associated with photoisomerization.[37] Additionally, we measured the fluorescence lifetime for the phenylacetylene-based molecules using picosecond pulses at 266 nm as excitation. We did not measure the fluorescence lifetime for **YB3p25** because our

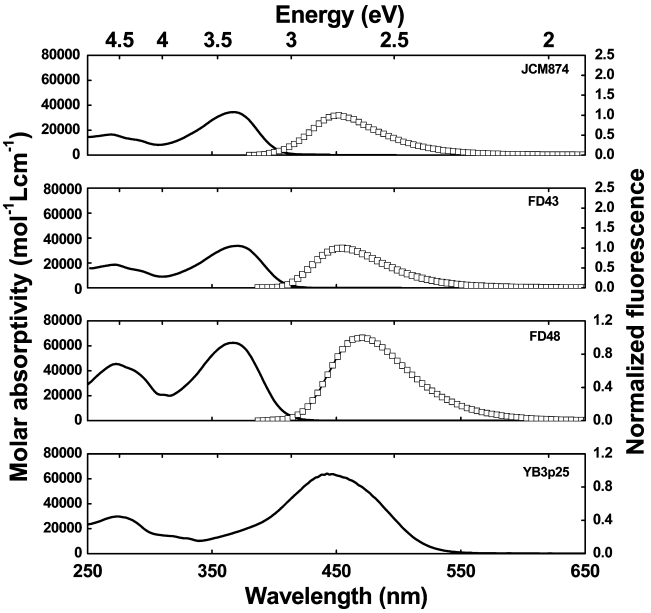


**Figure 1.** Molar absorptivity (solid lines) and fluorescence spectra (square) of, from top to bottom, compounds **JCM874**, **FD43**, **FD48**, and **YB3p25** in chloroform solutions.

experimental setup does not have enough sensitivity. The deconvoluted fluorescence decay curves as well as the lifetime values obtained by using the deconvolution method are shown in Figure 2. The solid lines show the fit obtained by using the deconvolution method described in the Experimental Section. As it can be seen, all molecules present fluorescence lifetimes on the order of 2 ns. By using the SB equation (see Experimental Section), we estimated the expected value to the fluorescence lifetime. Table 1 shows the calculated ($\tau_f^{SB}$) and experimental ($\tau_f^{exp}$) fluorescence lifetimes for **JCM874**, **FD43**,and **FD48**. A good agreement is observed, within the experimental error, between the calculated and experimental fluorescence lifetimes.

Figure 3 shows the experimental 2PA spectra (empty circles) determined by performing open-aperture Z-scan measurements with femtosecond pulses. In Figure 4 we present experimental Z-scan curves and the corresponding 2PA fit[38] for all studied molecules at the wavelength of the peak of the lowest energy 2PA bands. From Z-scan curves similar to these, at distinct excitation wavelengths, we obtained the dependence of the 2PA cross-section with the wavelength shown in Figure 3. For all molecules, the experimental nonlinear spectrum presents the intermediate state resonance enhancement effect,[39,40] as well as two 2PA allowed bands. These bands correspond to a transition to a excited state, which is also one-photon absorption (1PA) allowed, located at the UV−visible region, accomplished by the absorption of two photons in the visible and near-infrared.

The cross-section values, at the peak of the 2PA allowed bands, were determined to be ca. 100 ± 20 GM at 540 nm and 80 ± 10 GM at 740 nm for compound **JCM874**; 130 ± 20 GM at 540 nm and 100 ± 10 GM at 750 nm for compound **FD43**; 250 ± 30 GM at 540 nm and 190 ± 20 GM at 740 nm for compound **FD48**; and 90 ± 10 GM at 660 nm and 230 ± 30 GM at 880 nm for compound **YB3p25** (see circles in Figure 3). Such 2PA cross-section values are in good agreement with the ones reported for molecules with similar structure.[41,42] It is observed that **FD48** has approximately 2 times higher 2PA cross-section than **FD43** and **JCM874**, which indicates an


dx.doi.org/10.1021/jp310731t | J. Phys. Chem. B 2012, 116, 14677−14688

**Table 1. Photophysical Data of the Investigated Compounds in Chloroform**

| molecules | $M_w$ (g/mol) | $\lambda_{max}^{abs}$(nm) | $\varepsilon_{max}$ ($mol^{-1}$ L $cm^{-1}$) | $\lambda_{max}^{emi}$(nm) | $\phi_{max}$ | $\tau_f^{exp}$(ns) | $\tau_f^{SB}$(ns) |
|---|---|---|---|---|---|---|---|
| **JCM874** | 483.73 | 368 | 34550 | 452 | 0.48 | 2.0 ± 0.3 | 1.60 ± 0.20 |
| **FD43** | 508.74 | 370 | 33680 | 454 | 0.61 | 2.1 ± 0.3 | 1.70 ± 0.20 |
| **FD48** | 889.30 | 367 | 64200 | 466 | 0.49 | 2.2 ± 0.3 | 1.95 ± 0.20 |
| **YB3p25** | 897.29 | 444 | 64600 | | | | |

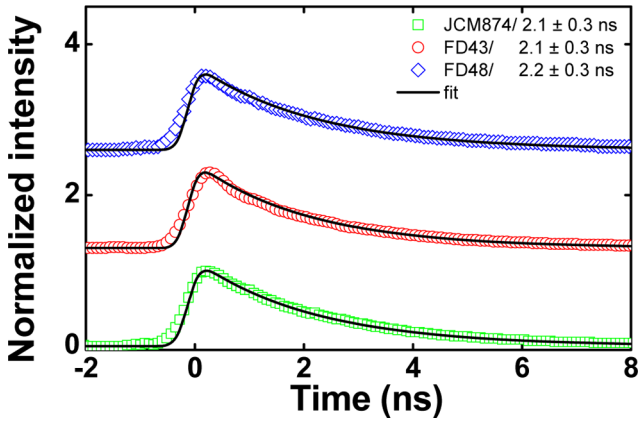


**Figure 2.** Time-resolved fluorescence for phenylacetylene derivatives obtained using picosecond excitation at 266 nm. The fluorescence lifetime was determined through the deconvolution method. The solid lines show the fit obtained by using the deconvolution method.

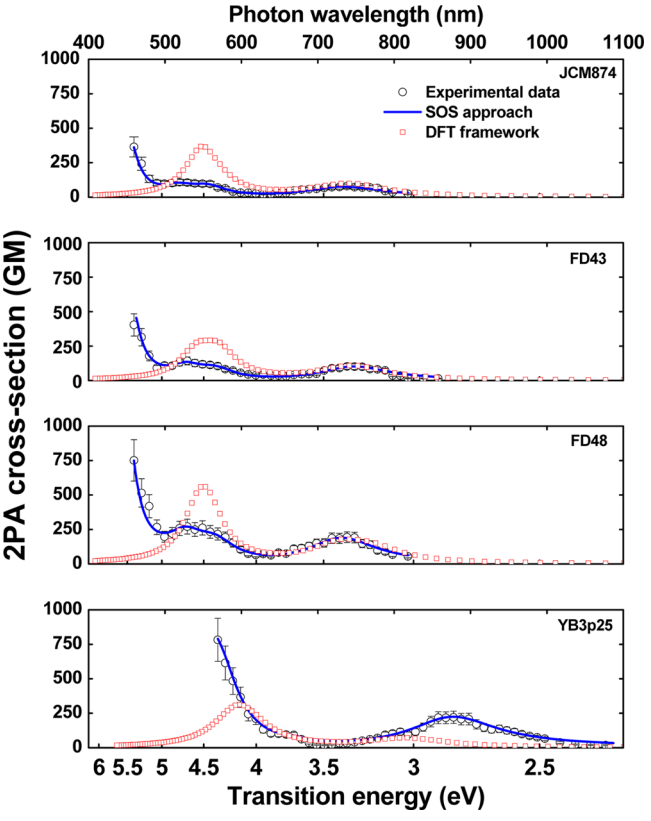


**Figure 3.** The circles represent the 2PA cross-section spectra, and the solid lines along it represent the theoretical fitting obtained employing the sum-over-essential states approach. The squares correspond to the theoretical 2PA cross-section spectra obtained using the results (transition energies and 2PA probabilities) of the quadratic response function calculations within the DFT framework (CAM-B3LYP/6-31+G(d)).

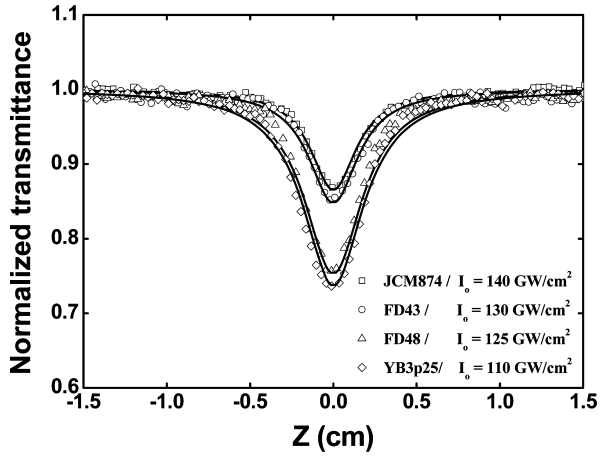


**Figure 4.** Open-aperture Z-scan curves for **JCM874** (squares), **FD43** (circles), **FD48** (triangles), and **YB3p25** (diamonds) in chloroform solution, at 740, 750, 740, and 870 nm, respectively. The solid line represents the fitting employing the theory described in ref 38. The inset shows the input irradiancies used during the measurements.

additive effect in the cross-section magnitude due to the increase in the number of conjugation branches in this molecule by a factor of 2. Through the result (not shown) of a quadratic response calculation performed over the structure of a single branch of **YB3p25**, the same additive effect was verified on such system. Therefore, we do not observe for **FD48** and **YB3p25** any electronic coupling between branches that could enhance their 2PA cross sections due to cooperative effects.[17] The similar molar absorptivities and 2PA cross sections of **FD43** and **JCM874** show that the distinct rings present in the molecular structure of these systems do not effectively affect their linear and nonlinear absorption.

To confirm the actual 2PA nature of the experimental results (Figure 3), we measured the dependence of the Z-scan normalized transmittance change ($\Delta T$) and fluorescence induced by 2PA as a function of the excitation irradiance. The slope derived from a linear fit (log–log scale) of $\Delta T$ or fluorescence intensity as a function of excitation intensity indicates the mechanism of absorption. The results depicted in Figure 5 show a slope of approximately 2.0 for fluorescence (**FD43**, **JCM874**, and **FD48**) and 1.0 for $\Delta T$ (**YB3p25**), indicating a pure 2PA process. Another important feature of **FD43**, **FD48**, and **YB3p25** is that they exhibit molecular chirality, and, therefore, electric quadrupole and magnetic dipole moments can contribute to their 2PA cross-sections.[43] However, normally, the electric dipole terms dominate the nonlinear effect, and those two contributions may only be measured/identified if the effects of the electric dipole term vanish or cancel, as is the case in nonlinear circular dichroism.[44]

To further characterize the studied molecules and support our interpretations of the 1PA and 2PA spectra, we performed theoretical calculations employing the response functions, as detailed in the Computational Details section. The linear and


dx.doi.org/10.1021/jp310731t | J. Phys. Chem. B 2012, 116, 14677–14688

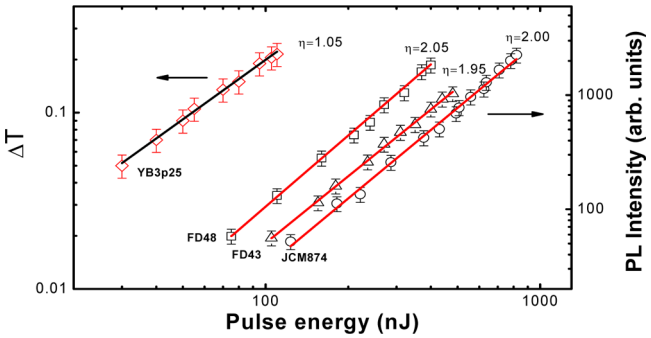


**Figure 5.** Transmittance change and PL intensity (log–log scale) as a function of pulse energy. A slope of approximately 1.0 at 870 nm was obtained for **YB3p25** using the Z-scan technique and ~2.0 at 740 nm for the phenylacetylene-based compounds using fluorescence excited by 2PA. These results confirm the two-photon nature of the nonlinear process.

quadratic response functions calculations were performed at the equilibrium molecular geometry of the molecules, shown in Figure 6, and allowed to determine their 20 lowest energy transitions for each compound.

In the equilibrium molecular geometry, the two aromatic rings of the backbone of **FD43** and **JCM874** and of each branch of the **FD48** and **YB3p25** stay in the same plane, which favors the delocalization of their $\pi$-electrons. Moreover, there is no $\pi-\pi$ stacking between the two branches of the **FD48** and **YB3p25** molecules. Through the results of additional response function calculations (data not shown), we verified that the lateral and saturated chains of the investigated compound do not play any role on their 1PA and 2PA spectroscopic properties. Table 2 presents the energy and intensity of the most intense 1PA and 2PA transitions of each molecule through the UV–vis. It is important to mention that it has been often shown that a B3LYP description for transitions with charge-transfer character is associated with a significant error. The spatial overlap ($\Lambda$) computed for a given excitation has been used as a diagnostic parameter for its charge-transfer character.[45] For all molecules studied here, the computed $\Lambda$ values for the transitions reported in Table 2 are between 0.35–0.60, which suggests that the usage of B3LYP functional is justified. As shown in Table 2, **JCM874** and **FD43** have three electronic transitions located at 380, 285, and 275 nm with moderate 2PA probabilities ($>10^4$ a.u.), while for **FD48** and **YB3p25** the results indicate four electronic transitions with moderate 2PA probabilities located at 387, 365, 279, and 274 nm and 422, 405, 306, and 298 nm, respectively.

The states accessed via two-photon transitions are also allowed by 1PA, as shown by the oscillator strengths larger than 0.01 obtained for such transitions (see Table 2). Such results indicate that the electric-dipole selection rules are relaxed for all molecules investigated since they do not have symmetry of inversion. The theoretical results also indicate that the 2PA

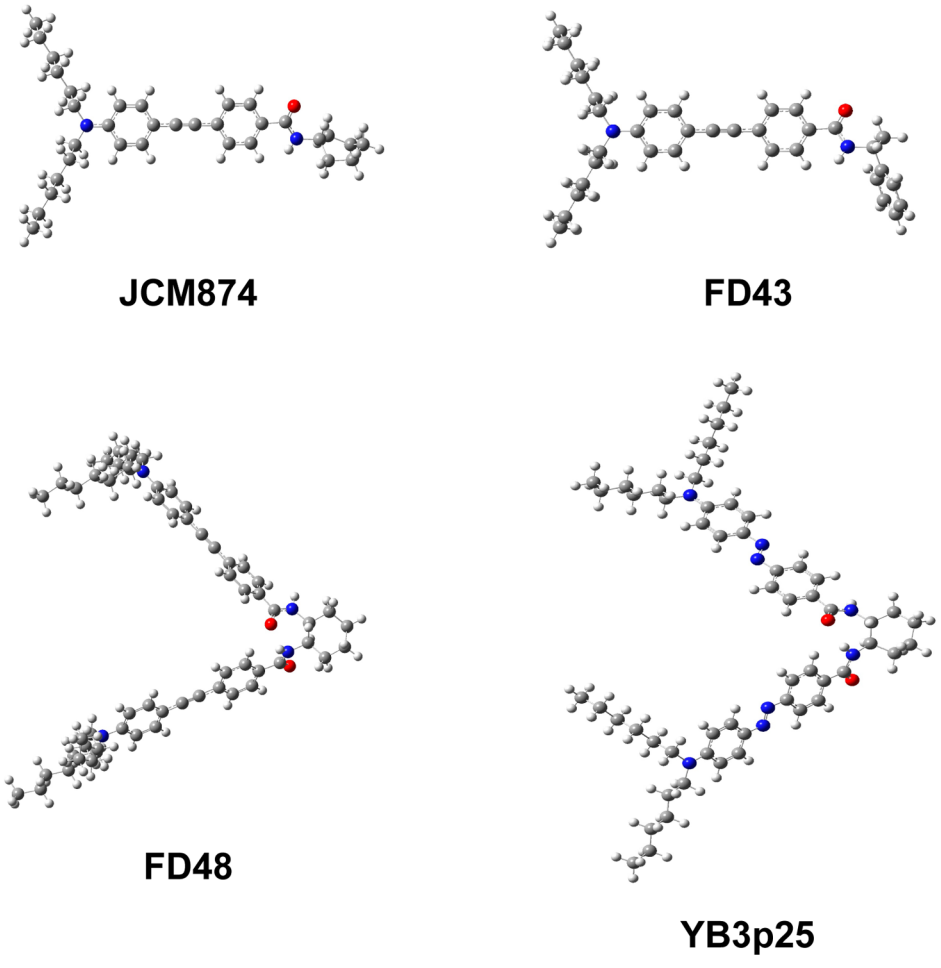


**Figure 6.** Equilibrium molecular geometry obtained by DFT calculations (B3LYP/6311G(d,p)).


dx.doi.org/10.1021/jp310731t | J. Phys. Chem. B 2012, 116, 14677–14688

**Table 2. Theoretical Results of the Energy and Intensity of the Most Important 1PA and 2PA Transitions of Each Compound Obtained Using Response Functions Calculations**[a]

| | 1PA | | 2PA | | |
|---|---|---|---|---|---|
| states | energy (eV) | oscillator strength | energy (eV) | transition probability (a.u.) | 2PA cross-section (GM) |
| **JCM874** | | | | | |
| $S_1$ ($\pi\pi^*$) | 3.30 (376 nm) | 1.290 | 3.30 (374 nm) | 70000 | 112.6 |
| $S_5$ ($\pi\pi^*$) | 4.37 (284 nm) | 0.047 | 4.37 (284 nm) | 16300 | 57.5 |
| $S_6$ ($\pi\pi^*$) | 4.48 (277 nm) | 0.375 | 4.48 (277 nm) | 106000 | 360.0 |
| **FD43** | | | | | |
| $S_1$ ($\pi\pi^*$) | 3.27 (379 nm) | 1.267 | 3.27 (379 nm) | 73300 | 115.8 |
| $S_5$ ($\pi\pi^*$) | 4.33 (286 nm) | 0.112 | 4.33 (286 nm) | 62000 | 214.7 |
| $S_8$ ($\pi\pi^*$) | 4.51 (275 nm) | 0.244 | 4.51 (275 nm) | 44000 | 165.3 |
| **FD48** | | | | | |
| $S_2$ ($\pi\pi^*$) | 3.20 (387 nm) | 1.087 | 3.20 (387 nm) | 53500 | 101.2 |
| $S_3$ ($\pi\pi^*$) | 3.40 (365 nm) | 1.478 | 3.40 (365 nm) | 50800 | 108.4 |
| $S_{16}$ ($\pi\pi^*$) | 4.43 (279 nm) | 0.335 | 4.43 (279 nm) | 70500 | 255.5 |
| $S_{19}$ ($\pi\pi^*$) | 4.53 (274 nm) | 0.261 | 4.53 (274 nm) | 95100 | 360.4 |
| **YB3p25** | | | | | |
| $S_4$ ($\pi\pi^*(n)$) | 2.94 (422 nm) | 0.814 | 2.94 (422 nm) | 17000 | 27.0 |
| $S_5$ ($\pi\pi^*(n)$) | 3.06 (405 nm) | 0.919 | 3.06 (405 nm) | 23400 | 40.2 |
| $S_{14}$ ($\pi\pi^*$) | 4.05 (306 nm) | 0.034 | 4.05 (306 nm) | 42200 | 126.7 |
| $S_{18}$ ($\pi\pi^*$) | 4.16 (298 nm) | 0.102 | 4.16 (298 nm) | 85600 | 217.2 |

[a]The 2PA cross sections were computed adopting linewidth values estimated through the fit of the nonlinear spectra.

band located around 270 nm in the experimental nonlinear spectrum of the phenylacetylene-based molecules (Figure 4) should be ascribed to two distinct 2PA allowed electronic states (Table 2) with moderate 2PA transition probabilities. Furthermore, in the case of **FD48** and **YB3p25**, which present a two-branch structure, the lowest energy 2PA band observed in Figure 3 should also be ascribed to two distinct 2PA allowed states. The oscillator strengths and the 2PA transition probabilities provided by the linear and quadratic response calculations confirm the similar linear and nonlinear optical properties of **FD43** and **JCM874**. The theoretical calculations also shed light on the linear and nonlinear optical properties of **FD48** and **YB3p25** and confirm the additive effect in these two-branch structures; however, the response calculations underestimated the oscillator strengths and the 2PA transition probabilities of **YB3p25**. The difference between the experimental and theoretical results obtained for **YB3p25** can, at least partially, be explained by the effect of the solvent environment on the optical properties of azoaromatic-based compounds. It is known that due to the existence of valence electron pairs without bonding (lone pairs) forming an n-type molecular orbital in these compounds,[46] solvent-induced polarization and conformational changes can substantially affect their linear and nonlinear optical properties. For **YB3p25**, the response calculations indicate that the n-type Kohn−Sham (KS) molecular orbital is involved in the electronic transitions to $S_1$ and $S_2$ states. However, in vacuo, such transitions do not have significant oscillator strength, and 2PA transition probabilities were not considered in the sum-over-essential states, which assumes only the most intense 2PA transitions (shown in Table 2) through the spectral region of interest. Therefore, for such compounds, a more realistic theoretical study, taking into account aspects such as solvent effects and conformational changes, seems to be needed for obtaining a better concordance between theoretical and experimental results.

The KS molecular orbitals involved in the excitation describing the single electronic transition corresponding to the lowest energy band in the 1PA and 2PA spectra of the **FD43** and **JCM874** molecules, or the two electronic transitions in the case of the **FD48** and **YB3p25** molecules, are shown in Figure 7. On the basis of the character of the KS molecular orbitals, one can conclude that all the transitions are $\pi\rightarrow\pi^*$ type. The one-electron excitations involved in the electronic transitions of **FD48** (transition 1: HOMO−1 → LUMO (93%) and HOMO → LUMO+1 (6%); transition 2: HOMO−1 → LUMO (6%) and HOMO → LUMO+1 (93%)) and **YB3p25** (transition1: HOMO−1 → LUMO (83%) and HOMO → LUMO+1 (15%); transition 2: HOMO−1 → LUMO (16%) and HOMO → LUMO+1 (83%)) do not indicate interbranch charge-transfer. Therefore, the $\pi\rightarrow\pi^*$ transitions observed in the lowest energy region of the 1PA and 2PA spectra of these two investigated molecules are not the charge-transfer type. However, for all investigated molecules, the $\pi\rightarrow\pi^*$ transitions observed in the lowest energy region of the spectra show a moderate intrabranch charge-transfer character.

To establish a relationship between the observed 2PA activity and molecular properties, we used the sum-over-essential states approach to analyze the experimental results presented in Figure 3. In most cases, a quantitative interpretation of the experimental 2PA cross-section spectrum can be accomplished taking into account only few-energy levels, since it is very difficult to obtain information about higher energy electronic states. In this case, as it is practically impossible to obtain all photophysical parameters from linear absorption measurements, the fit of the nonlinear absorption spectrum can provide important parameters concerning the electronic structure of organic molecules. On the basis of this statement, one can obtain an analytical expression for the 2PA cross-section employing the semiclassical time-dependent perturbation theory considering a few-energy-level diagram where the excited state energies were adopted based on the 2PA spectra and the results of the quantum chemical calculations (shown in Table 2). As the molecules studied here do not present a center of inversion, the initial and intermediate electronic states have distinct permanent dipole moments. Thus, it is necessary to take into account the real intermediate energy level. Additionally, noncentrosymmetric molecules do not follow the dipole-electric selection rule,[47] and, therefore, one- and two-photon transitions are allowed between any electronic states as shown by the results of the quantum chemical calculations. In this case, we can divide the 2PA spectrum into two parts. The first one corresponds to an electronic transition from the ground state to the 2PA allowed lowest-energy state with a change of permanent dipole moment (two-level system). For this dipolar


dx.doi.org/10.1021/jp310731t | J. Phys. Chem. B 2012, 116, 14677−14688

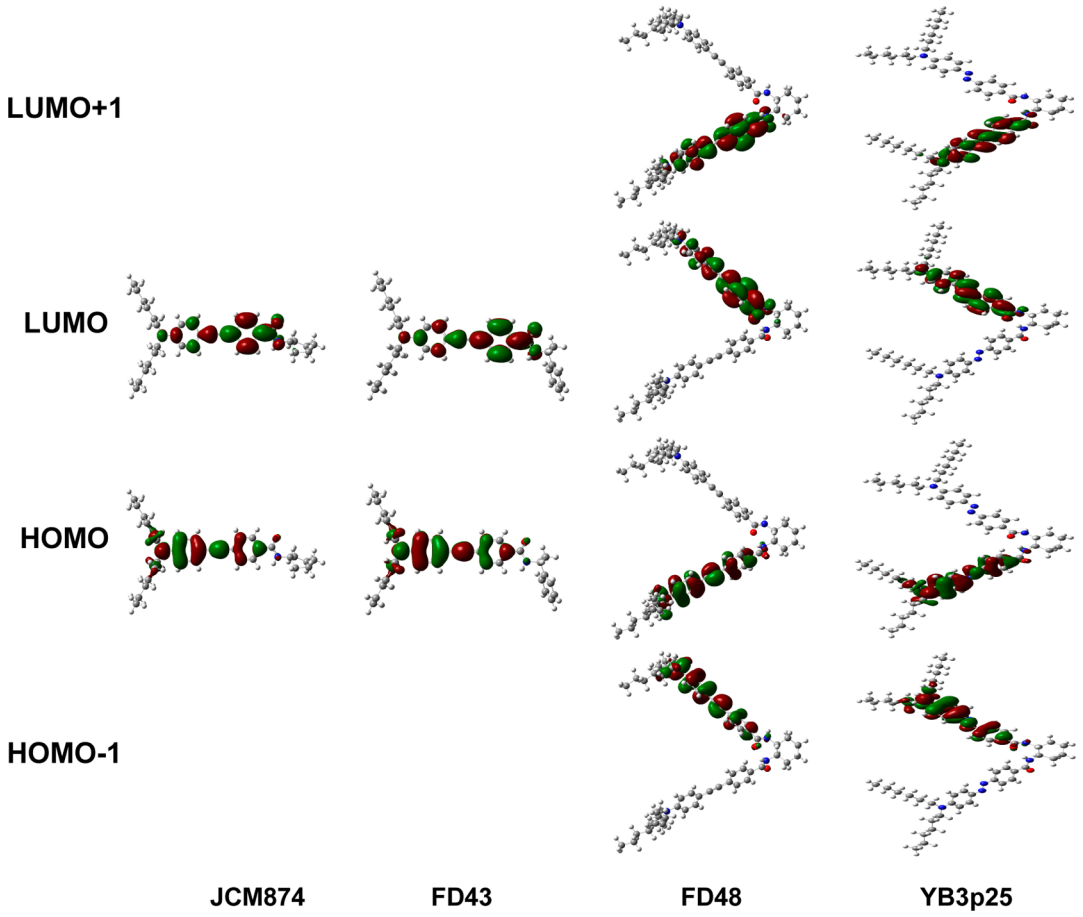


**Figure 7.** KS molecular orbitals involved in the excitations describing the electronic transitions responsible for the lowest energy bands in the 1PA and 2PA spectra.

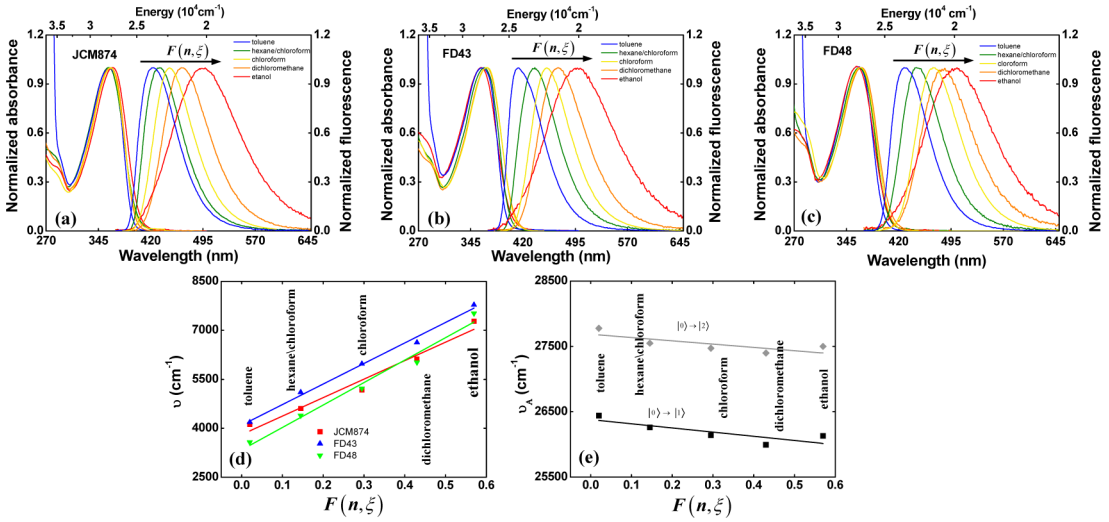


**Figure 8.** Normalized absorption and fluorescence spectra of the (a) **JCM874**, (b) **FD43**, and (c) **FD48** in five different solvents (toluene, hexane/chloroform, chloroform, dichloromethane, and ethanol). (d) Solvatochromic Stoke shift ($\upsilon$) measurements obtained as a function of the Onsager polarity function ($F(n,\xi)$). (e) Solvatochromic shift measurements as a function of the Onsager polarity of solvent for the lowest energy band of the **FD48** molecule shown in panel c.

contribution (two-level system), taking into account the average over all possible molecular orientations in an isotropic medium and assuming linearly polarized light and that the dipole moments are parallel, the 2PA cross-section can be written as[39,48]

$$\sigma_{g\to f}^{(2PA)}(\omega) = \frac{2}{5}\frac{(2\pi)^5}{(nhc)^2}L^4|\vec{\mu}_{gf}|^2|\Delta\vec{\mu}_{gf}|^2 g_{g\to f}(2\omega) \quad (3)$$

where $h$ is Planck's constant, $c$ is the speed of light, $L = 3n^2/(2n^2 + 1)$ is the Onsager local field factor introduced to take


dx.doi.org/10.1021/jp310731t | J. Phys. Chem. B 2012, 116, 14677−14688

into account the medium effect with $n = 1.49$ for chloroform. $\vec{\mu}_{gf}$ is the transition dipole moment vector from ground to final excited state, $\Delta\vec{\mu}_{gf}$ is the difference between the permanent dipole moments vectors of the excited ($\vec{\mu}_{ff}$) and ground ($\vec{\mu}_{gg}$) states. $g_{g\rightarrow f}(2\omega)$ represents the normalized line-shape function of the excited state, and in this paper we assumed it as a Gaussian function given by

$$g_{g\rightarrow f}(2\omega) = \frac{1}{\pi}\frac{\Gamma_{gf}/2}{(\omega_{gf} - 2\omega)^2 + (\Gamma_{gf}/2)^2} \tag{4}$$

where $\Gamma_{gf}$ is the damping constant describing the FWHM of the final state line width (assuming Lorentzian line-shape). In eq 3 the normalized line-shape function $g_{gf}(\omega)$and transition dipole moment $|\vec{\mu}_{gf}|$ can be evaluated directly from the molar absorptivity spectrum using the following equation:

$$|\vec{\mu}_{gf}|^2 g_{gf}^{\max} = \frac{3\times 10^3 \ln(10)hc}{(2\pi)^2 N_A}\frac{n}{L^2}\frac{\varepsilon_{\max}(\omega_{gf})}{\omega_{gf}} \tag{5}$$

where $\varepsilon_{\max}(\omega_{gf})$ is the peak molar absorptivity corresponding at maximum transition frequency $\omega_{gf}$, and $N_A$ is Avogadro's number. The permanent dipole moment change, $|\Delta\vec{\mu}_{01}|$, can be obtained, in the dipole−dipole interaction, from solvatochromic shift measurements given by

$$|\Delta\vec{\mu}_{01}|^2 = hc\frac{\partial\upsilon}{\partial F}a^3 \tag{6}$$

where $\upsilon = \upsilon_A - \upsilon_{em}$ is the difference between the wavenumber of the maximum absorption and fluorescence emission (in $cm^{-1}$). $F(n,\xi) = (\xi - 1)/(2\xi + 1) - (n^2 - 1)/(2n^2 + 1)$ is the Onsager polarity function, with $\xi$ being the dielectric constant of the solvent. $a$ is the radius of the molecular cavity, assumed to be spherical. We performed solvatochromic measurements for **JCM874**, **FD43**, and **FD48** molecules in five different solvents (toluene, hexane/chloroform (50−50%), chloroform, dichloromethane and ethanol), as shown in Figure 8. We did not measure the solvatochromic shift for **YB3p25** because its fluorescence quantum yield is too low. Proceeding in this way, we obtained $(\partial\upsilon_{JCM874})/(\partial F) = 5660 \pm 600\ cm^{-1}$, $(\partial\upsilon_{FD43})/(\partial F) = 6880 \pm 400\ cm^{-1}$, and $(\partial\upsilon_{FD48})/(\partial F) = 6290 \pm 600\ cm^{-1}$. Assuming $a$ as 40% of the $\pi$-conjugated backbone maximum length of the molecules[49] ($a_{JCM874} = a_{FD43} = 5.1$ Å and $a_{FD48} = 5.6$ Å), we found $|\Delta\vec{\mu}_{01}^{JCM874}| = 11.8 \pm 1.0D$, $|\Delta\vec{\mu}_{01}^{FD43}| = 13.1 \pm 1.0D$ and $|\Delta\vec{\mu}_{01}^{FD48}| = 14.5 \pm 0.6D$.

To model the higher energy 2PA allowed states we considered a three-level energy system in which it is considered the ground state, one intermediate 1PA allowed excited state ($|1\rangle$) and the 2PA allowed final excited state. For this system, the 2PA cross-section can be written as (assuming linearly polarized light and that the dipole moments are parallel)[39,48,50]

$$\sigma_{g\rightarrow f}^{(2PA)}(\omega) = \frac{2}{5}\frac{(2\pi)^5}{(nhc)^2}L^4\left\{|\vec{\mu}_{0f}|^2|\Delta\vec{\mu}_{0f}|^2 + R(\omega)|\vec{\mu}_{01}|^2|\vec{\mu}_{1f}|^2 + 2R(\omega)\frac{(\omega_{01} - \omega)}{\omega}|\vec{\mu}_{01}||\vec{\mu}_{1f}||\vec{\mu}_{0f}||\Delta\vec{\mu}_{0f}|\right\} g_{g\rightarrow f}(2\omega) \tag{7}$$

where $\omega$ is the excitation laser, $\vec{\mu}_{1f}$ is the transition dipole moment between the excited states $|1\rangle \rightarrow |f\rangle$, and $R(\omega) = \omega^2/[(\omega_{01} - \omega)^2 + \Gamma_{01}^2(\omega)]$ is the resonance enhancement factor.

As it can be seen from eq 7, the 2PA cross-section in a three-energy level system is governed by three contributions: the first corresponds to a 2PA transition in a two-level system with a change of permanent dipole moment ($\Delta\vec{\mu}_{0f} \neq 0$), while the second contribution corresponds to transitions in a three-level system with one final excited state and one intermediate real excited state ($|1\rangle$), which is responsible for resonance enhancement of the nonlinearity. The last contribution corresponds to interference between the two excitation pathways. However, if the photon energy is very close to the intermediate real state ($|1\rangle$), the 2PA cross-section described by eq 7 can be rewritten as

$$\sigma_{g\rightarrow f}^{(2PA)}(\omega) = \frac{2}{5}\frac{(2\pi)^5}{(nhc)^2}L^4R(\omega)|\vec{\mu}_{01}|^2|\vec{\mu}_{1f}|^2 g_{g\rightarrow f}(2\omega) \tag{8}$$

since the second term of eq 5 becomes much stronger than the first ($R(\omega)|\vec{\mu}_{01}|^2|\vec{\mu}_{1f}|^2 \gg |\vec{\mu}_{0f}|^2|\Delta\vec{\mu}_{0f}|^2$) due to the resonance enhancement factor and because, in this situation ($\omega \rightarrow \omega_{01}$), the contribution of the interference term to the total 2PA cross-section is very small.

As can be seen in eq 7, the 2PA cross-section in a three-energy level system depends on the four distinct dipole moments ($|\vec{\mu}_{01}|$, $|\vec{\mu}_{0f}|$, $|\Delta\vec{\mu}_{0f}|$, and $|\vec{\mu}_{1f}|$). The dipole moments $|\vec{\mu}_{01}|$ and $|\vec{\mu}_{0f}|$ can be obtained from eq 5. However, eq 6 can be applied only to the lowest-energy transition, and, therefore, $|\Delta\vec{\mu}_{0f}|$ cannot be obtained directly by it. In this case, for higher energy transitions, one can use eq 9, which relates the shift of the maximum absorption ($\upsilon_A(cm^{-1})$) with the solvent polarity ($F(n,\xi)$):[49]

$$\Delta\vec{\mu}_{0f}\cdot\vec{\mu}_{00} = -hc\frac{\partial\upsilon_A}{\partial F}a^3 \tag{9}$$

where $\mu_{00}$ is the permanent dipole moment in the ground state. We used eq 9 to obtain the $|\Delta\vec{\mu}_{02}|$ for **FD48** since its lowest energy 2PA allowed band is described by two electronic transitions with similar 2PA probabilities. From the solvatochromic measurements shown in Figure 8e, we obtained $(\partial\upsilon_A^{FD48})/(\partial F) = -660 \pm 190\ cm^{-1}$ for the transition $|0\rangle \rightarrow |1\rangle$ and $(\partial\upsilon_A^{FD48})/(\partial F) = -510 \pm 150\ cm^{-1}$ for the transition $|0\rangle \rightarrow |2\rangle$. Proceeding in this way, we obtained $|\vec{\mu}_{00}^{FD48}| = 1.65 \pm 0.65D$ assuming that the angle between the dipole moments ($|\vec{\mu}_{00}^{FD48}|$ and $|\vec{\mu}_{02}^{FD48}|$) is approximately zero and, consequently, found $|\Delta\vec{\mu}_{02}^{FD48}| = 10.5 \pm 2.5D$.

As the fluorescence quantum yield of the **YB3p25** is too low and its lowest energy 2PA band is ascribed to the overlapping of two electronic states, as pointed out by the theoretical calculations, we used the 2PA probabilities to weight the contribution of each excited state separately. Table 3 summarizes the spectroscopic parameters used/obtained in the sum-over-essential states approach employed to model the 2PA spectra. It is important to emphasize that the electronic states used in the sum-over-essential states (Table 3) correspond to the most important 2PA allowed transitions identified through the quadratic response calculations (shown in Table 2). Therefore, for the **JCM874** and **FD43**, the states labeled as the $|1\rangle$, $|2\rangle$, and $|3\rangle$ in the sum-over-essential states correspond, respectively, to the $S_1$, $S_5$, and $S_6$ (or $S_8$ for the **FD43**) states identified by the theoretical calculations; while for the **FD48** and **YB3p25**, the excited states labeled as the $|1\rangle$, $|2\rangle$, $|3\rangle$, and $|4\rangle$ in the sum-over-essential correspond to the $S_2$, $S_3$, $S_{16}$, and $S_{19}$ states and $S_4$, $S_5$, $S_{14}$, and $S_{18}$ states, respectively.


dx.doi.org/10.1021/jp310731t | J. Phys. Chem. B 2012, 116, 14677−14688

**Table 3. Spectroscopic Parameters Used/Obtained (Highlight) in/from the Sum-Over-Essential States Approach Adopting a Few-Energy-Levels Diagram[a]**

| 2PA parameters | JCM874 | FD43 | FD48 | YB3p25 |
|---|---|---|---|---|
| $\lambda_{01}$ (nm) | 368 (3.37 eV) | 373 (3.33 eV) | 375 (3.30 eV) | 460 (2.70 eV) |
| $\lambda_{02}$ (nm) | 280 (4.43 eV) | 285 (4.35 eV) | 360 (3.44 eV) | 435 (2.85 eV) |
| $\lambda_{03}$ (nm) | 260 (4.77 eV) | 265 (4.68 eV) | 285 (4.35 eV) | 335 (3.70 eV) |
| $\lambda_{04}$ (nm) | 225 (5.51 eV) | 225 (5.51 eV) | 265 (4.68 eV) | 285 (4.35 eV) |
| $\lambda_{05}$ (nm) | | | 230 (5.39 eV) | |
| $\Gamma_{01}$ (eV) | 0.50 ± 0.05 | 0.50 ± 0.05 | 0.40 ± 0.05 | 0.40 ± 0.05 |
| $\Gamma_{02}$ (eV) | 0.42 ± 0.05 | 0.40 ± 0.05 | 0.40 ± 0.05 | 0.40 ± 0.05 |
| $\Gamma_{03}$ (eV) | 0.42 ± 0.05 | 0.40 ± 0.05 | 0.42 ± 0.05 | 0.50 ± 0.05 |
| $\Gamma_{04}$ (eV) | 0.54 ± 0.05 | 0.54 ± 0.05 | 0.42 ± 0.05 | 0.5 ± 0.05 |
| $\Gamma_{05}$ (eV) | | | 0.54 ± 0.05 | |
| $\mu_{01}$ (D) | 8.60 ± 1.0 | 8.50 ± 1.0 | 8.50 ± 1.0 | 8.70 ± 1.0 |
| $\mu_{02}$ (D) | 3.50 ± 0.5 | 4.00 ± 0.5 | 9.50 ± 1.0 | 9.50 ± 1.0 |
| $\mu_{12}$ (D) | 4.0 ± 1.0 | 4.5 ± 0.5 | 2.5 ± 0.5 | 9.0 ± 2.0 |
| $\mu_{13}$ (D) | 4.0 ± 1.0 | 5.0 ± 0.5 | 9.0 ± 2.0 | 0.5 ± 0.2 |
| $\mu_{14}$ (D) | 7.0 ± 1.0 | 8.0 ± 1.0 | 6.5 ± 1.0 | 8.5 ± 1.0 |
| $\mu_{15}$ (D) | | | 7.5 ± 1.0 | |
| $\Delta\mu_{01}$ (D) | 12.0 ± 2.0 | 13.0 ± 2.0 | 12.0 ± 2.0 | 10.5 ± 2.0 |
| $\Delta\mu_{02}$ (D) | 6.0 ± 2.0 | 6.0 ± 2.0 | 9.0 ± 2.0 | 6.0 ± 2.0 |

[a] $\Gamma_{gf}$ is the damping constant describing FWHM of the final excited state line-shape function (a Lorentzian function) and $\lambda_{fg} = 2\pi c/\omega_{fg}$. The excited states for the **JCM874** and **FD43** molecules labeled here as $|1\rangle$, $|2\rangle$, and $|3\rangle$ states correspond, respectively, to the $S_1$, $S_5$, and $S_6$ (or $S_8$ for the FD43 molecule) states identified by the theoretical calculations (Table 2). For the **FD48** and **YB3p25** molecules, the excited states labeled here as the $|1\rangle$, $|2\rangle$, $|3\rangle$, and $|4\rangle$ states correspond to the $S_2$, $S_3$, $S_{16}$, and $S_{19}$ states and $S_4$, $S_5$, $S_{15}$, and $S_{20}$ states, respectively.

To further compare the experimental and theoretical 2PA results, we simulated the 2PA cross-section spectra assuming a spectral line function for each of the main 2PA allowed transitions (reported in Table 2) among the 20 lowest energy transitions determined and performing a convolution of such functions. The linewidths adopted for such Lorentzian functions are shown in Table 3 and were estimated by fitting the experimental nonlinear spectra using the sum-over-essential states approach. The amplitude adopted for each spectral line function is the theoretical estimate of the 2PA cross-section of each excited state showed in Table 2. As it can be seen, there is a good agreement between theoretical and experimental results concerning the spectral profile of the nonlinear spectra, as well as the 2PA cross-section magnitude for all investigated molecules. However, considerable differences are observed between the experimental and theoretical 2PA cross-section magnitude at the higher energy region (>4 eV) of the nonlinear spectrum. Such differences are, most probably, due to the imprecision in the determination of the linewidths in this region with the high density of electronic states.

As previously mentioned, the relationship between chemical structures and photophysical parameters is important to determine 2PA properties of organic chromophores. In this context, we also performed linear and quadratic response function calculations to determine the transition dipole moment and permanent dipole moment change of two lowest-energy transitions strongly allowed by 2PA (see Table 4). We compared these theoretical results with the values obtained using the sum-over-essential states approach and solvatochromic measurements (see Table 4) and observed a good agreement. Such agreement shows that there is a strong correlation between the experimental and theoretical results, reinforcing that response function calculations within the DFT framework can be used to provide valuable information about the electronic structure of novel 2PA absorbing materials assisting in their development.

## V. FINAL REMARKS

1PA and 2PA properties of four molecules containing $\pi$-conjugated backbone based on phenylacetylene (**JCM874**, **FD43** and **FD48**) and azoaromatic (**YB3p25**) moieties were investigated using experimental and theoretical methods. The results showed that these molecules present considerable molar absorptivity in the UV (phenylacetylene) and visible (azoaromatic) region, accompanied by 2PA cross-section on the order of a few hundreds of GM in the visible (phenylacetylene) and NIR-IR (azoaromatic). We observed, along the nonlinear spectra, two 2PA allowed bands that correspond to transitions to one-photon allowed states, indicating relaxation of the dipole-electric selection rules. In addition, we observed for all molecules the resonance enhancement effect, providing, for shorter wavelengths, a significant enhancement of the 2PA of approximately 4 times in comparison to the dipolar transition, which does not involve any intermediate state. We interpreted the 2PA spectrum, based on the results of response function calculations and, in addition, their spectral behavior was modeled using a few-level-energy diagram within the sum-over-essential states. We observed a strong correlation between the experimental and theoretical results for magnitude, spectral behavior, and photophysical parameters involved in 2PA, indicating that both methods provided powerful and comple-

**Table 4. Comparison between the Values Estimated for the Photophysical Parameters of the Compounds Investigated through the Fitting of the Experimental 2PA Spectra (Labeled as "exp" Values), Solvatochromic Shift Measurements (Labeled as "SS" Values), and the Values Provided by the Theoretical Calculations (Labeled as "theo" Values)[a]**

| compounds | $\vec{\mu}_{01}^{theo}$ | $\vec{\mu}_{01}^{exp}$ | $\vec{\mu}_{01}^{theo}$ | $\vec{\mu}_{01}^{exp}$ | $\vec{\mu}_{01}^{SS}$ | $\vec{\mu}_{02}^{theo}$ | $\vec{\mu}_{02}^{exp}$ | $\vec{\mu}_{02}^{theo}$ | $\vec{\mu}_{02}^{exp}$ | $\vec{\mu}_{02}^{SS}$ |
|---|---|---|---|---|---|---|---|---|---|---|
| **JCM874** | 10.83 | 8.54 | 14.64 | 12.00 | 11.80 | 1.7 | 3.5 | 14.62 | 6.00 | |
| **FD43** | 10.10 | 8.46 | 14.60 | 13.00 | 13.10 | 2.6 | 4.0 | 5.86 | 6.00 | |
| **FD48** | 9.12 | 8.50 | 14.14 | 12.00 | 14.50 | 10.63 | 9.50 | 12.30 | 9.00 | 10.50 |
| **YB3p25** | 8.54 | 8.70 | 5.89 | 10.50 | | 8.90 | 9.50 | 5.50 | 6.00 | |

[a] The excited states for the **JCM874** and **FD43** molecules labeled here as $|1\rangle$ and $|2\rangle$ states correspond, respectively, to the $S_1$ and $S_5$ states identified by the theoretical calculations (Table 2). For the **FD48** and **YB3p25** molecules, the excited states labeled here as the $|1\rangle$ and $|2\rangle$ states correspond to the $S_2$ and $S_3$ states and $S_4$ and $S_5$ states, respectively.


dx.doi.org/10.1021/jp310731t | J. Phys. Chem. B 2012, 116, 14677−14688

mentary information concerning the electronic structure of organic materials.

## ■ ASSOCIATED CONTENT

### Supporting Information

General experimental information, preparation of compound 3−5, and copies of $^{1}H$ and $^{13}C$ spectra for compounds **2**, **5**, **6**, **YB3p25**, **FD48**, **FD43**, and **JCM874**. Theoretical information about the atom coordinates and absolute energies for compounds **YB3p25**, **FD48**, **FD43**, and **JCM874** are also reported. This material is available free of charge via the Internet at http://pubs.acs.org.

## ■ AUTHOR INFORMATION

### Corresponding Author

*E-mail: mavivas82@yahoo.com.br (M.G.V.); crmendon@ifsc.usp.br (C.R.M.).

### Notes

The authors declare no competing financial interest.

## ■ ACKNOWLEDGMENTS

Financial support from FAPESP (Fundação de Amparo à Pesquisa do estado de São Paulo), CNPq (Conselho Nacional de Desenvolvimento Científico e Tecnológico), Coordenaçao de Aperfeiçoamento de Pessoal de Nível Superior (CAPES), and the Air Force Office of Scientific Research are acknowledged. The authors also gratefully acknowledge the allotment of the CPU time in Wrocław Center of Networking and Supercomputing (WCSS). One of the authors (R.Z.) is beneficiary of the KOLUMB fellowship funded by the Foundation for Polish Science (FNP).

## ■ REFERENCES

(1) Corredor, C. C.; Huang, Z. L.; Belfield, K. D. *Adv. Mater.* **2006**, *18*, 2910−2914.
(2) Denk, W.; Strickler, J. H.; Webb, W. W. *Science* **1990**, *248*, 73−76.
(3) McIlroy, S. P.; Clo, E.; Nikolajsen, L.; Frederiksen, P. K.; Nielsen, C. B.; Mikkelsen, K. V.; Gothelf, K. V.; Ogilby, P. R. *J. Org. Chem.* **2005**, *70*, 1134−1146.
(4) Tsiminis, G.; Ribierre, J. C.; Ruseckas, A.; Barcena, H. S.; Richards, G. J.; Turnbull, G. A.; Burn, P. L.; Samuel, I. D. W. *Adv. Mater.* **2008**, *20*, 1940−1944.
(5) Ehrlich, J. E.; Wu, X. L.; Lee, I. Y. S.; Hu, Z. Y.; Rockel, H.; Marder, S. R.; Perry, J. W. *Opt. Lett.* **1997**, *22*, 1843−1845.
(6) Ferreira, P. H. D.; Vivas, M. G.; Silva, D. L.; Misoguti, L.; Feng, K.; Bu, X. R.; Mendonca, C. R. *Opt. Commun.* **2011**, *284*, 3433−3436.
(7) Mendonca, C. R.; Cerami, L. R.; Shih, T.; Tilghman, R. W.; Baldacchini, T.; Mazur, E. *Opt. Express* **2008**, *16*, 200−206.
(8) Correa, D. S.; Cardoso, M. R.; Tribuzi, V.; Misoguti, L.; Mendonca, C. R. *IEEE J. Sel. Top. Quant.* **2012**, *18*, 176−186.
(9) Katan, C.; Terenziani, F.; Mongin, O.; Werts, M. H. V.; Porres, L.; Pons, T.; Mertz, J.; Tretiak, S.; Blanchard-Desce, M. *J. Phys. Chem. A* **2005**, *109*, 3024−3037.
(10) Makarov, N. S.; Rebane, A.; Drobizhev, M.; Wolleb, H.; Spahni, H. *J. Opt. Soc. Am. B* **2007**, *24*, 1874−1885.
(11) Vivas, M. G.; Silva, D. L.; De Boni, L.; Zalesny, R.; Bartkowiak, W.; Mendonca, C. R. *J. Appl. Phys.* **2011**, *109*, 103529-1−103529-8.
(12) Lee, S.; Thomas, K. R. J.; Thayumanavan, S.; Bardeen, C. J. *J. Phys. Chem. A* **2005**, *109*, 9767−9774.
(13) Vivas, M. G.; Silva, D. L.; Misoguti, L.; Zalesny, R.; Bartkowiak, W.; Mendonca, C. R. *J. Phys. Chem. A* **2010**, *114*, 3466−3470.
(14) Wang, X. M.; Wang, D.; Zhou, G. Y.; Yu, W.; Zhou, Y. T.; Fang, Q. F.; Jiang, M. H. *J. Mater. Chem.* **2001**, *11*, 1600−1605.
(15) Hales, J. M.; Matichak, J.; Barlow, S.; Ohira, S.; Yesudas, K.; Bredas, J. L.; Perry, J. W.; Marder, S. R. *Science* **2010**, *327*, 1485−1488.
(16) Marder, S. R.; Perry, J. W.; Bourhill, G.; Gorman, C. B.; Tiemann, B. G.; Mansour, K. *Science* **1993**, *261*, 186−189.
(17) Drobizhev, M.; Karotki, A.; Dzenis, Y.; Rebane, A.; Suo, Z. Y.; Spangler, C. W. *J. Phys. Chem. B* **2003**, *107*, 7540−7543.
(18) De Boni, L.; Piovesan, E.; Misoguti, L.; Zilio, S. C.; Mendonca, C. R. *J. Phys. Chem. A* **2007**, *111*, 6222−6224.
(19) Vivas, M. G.; Mendonca, C. R. *J. Phys. Chem. A* **2012**, *116*, 7033−7038.
(20) Kim, H. M.; Lee, Y. O.; Lim, C. S.; Kim, J. S.; Cho, B. R. *J. Org. Chem.* **2008**, *73*, 5127−5130.
(21) De Boni, L.; Misoguti, L.; Zilio, S. C.; Mendonca, C. R. *ChemPhysChem* **2005**, *6*, 1121−1125.
(22) Varnavski, O.; Yan, X. Z.; Mongin, O.; Blanchard-Desce, M.; Goodson, T. *J. Phys. Chem. C* **2007**, *111*, 149−162.
(23) Kohn, W.; Sham, L. J. *Phys. Rev.* **1965**, *140*, A1133−A1138.
(24) Birge, R. R.; Pierce, B. M. *J. Chem. Phys.* **1979**, *70*, 165−178.
(25) Rebane, A.; Drobizhev, M.; Makarov, N. S.; Beuerman, E.; Haley, J. E.; Douglas, M. K.; Burke, A. R.; Flikkema, J. L.; Cooper, T. M. *J. Phys. Chem. A* **2011**, *115*, 4255−4262.
(26) Day, P. N.; Nguyen, K. A.; Pachter, R. *J. Phys. Chem. B* **2005**, *109*, 1803−1814.
(27) Teerenstra, M. N.; Hagting, J. G.; Schouten, A. J.; Nolte, R. J. M.; Kauranen, M.; Verbiest, T.; Persoons, A. *Macromolecules* **1996**, *29*, 4876−4879.
(28) Vivas, M. G.; Nogueira, S. L.; Silva, H. S.; Neto, N. M. B.; Marletta, A.; Serein-Spirau, F.; Lois, S.; Jarrosson, T.; De Boni, L.; Silva, R. A.; et al. *J. Phys. Chem. B* **2011**, *115*, 12687−12693.
(29) Cohen, B.; Crespo-Hernandez, C. E.; Kohler, B. *Faraday Discuss.* **2004**, *127*, 137−147.
(30) Strickler, S. J.; Berg, R. A. *J. Chem. Phys.* **1962**, *37*, 814−822.
(31) Becke, A. D. *J. Chem. Phys.* **1993**, *98*, 5648−5652.
(32) Lee, C. T.; Yang, W. T.; Parr, R. G. *Phys. Rev. B* **1988**, *37*, 785−789.
(33) Frisch, M. J.; Pople, J. A.; Binkley, J. S. *J. Chem. Phys.* **1984**, *80*, 3265−3269.
(34) Frisch, M. J.; Trucks, G. W.; Schlegel, H. B.; Scuseria, G. E.; Robb, M. A.; Cheeseman, J. R.; Montgomery, J. A.; Jr.; Vreven, T.; Kudin, K. N.; Burant, J. C. et al. *Gaussian 03*; Gaussian Inc.: Pittsburgh, PA, 2003.
(35) DALTON, A molecular electronic structure program, Release 2.0 (2005). See http://www.kjemi.uio.no/software/dalton/dalton.html, 2005.
(36) Silva, D. L.; Krawczyk, P.; Bartkowiak, W.; Mendonca, C. R. *J. Chem. Phys.* **2009**, *131*, 244516.
(37) Wang, L.; Xu, W.; Yi, C.; Wang, X. *J. Mol. Graph. Model.* **2009**, *27*, 792−796.
(38) Correa, D. S.; De Boni, L.; Misoguti, L.; Cohanoschi, I.; Hernandez, F. E.; Mendonca, C. R. *Opt. Commun.* **2007**, *277*, 440−445.
(39) Kamada, K.; Ohta, K.; Iwase, Y.; Kondo, K. *Chem. Phys. Lett.* **2003**, *372*, 386−393.
(40) Vivas, M. G.; Piovesan, E.; Silva, D. L.; Cooper, T. M.; De Boni, L.; Mendonca, C. R. *Opt. Mater. Express* **2011**, *1*, 700−710.
(41) De Boni, L.; Andrade, A. A.; Yamaki, S. B.; Misoguti, L.; Zilio, S. C.; Atvars, T. D. Z.; Mendonca, C. R. *Chem. Phys. Lett.* **2008**, *463*, 360−363.
(42) Chia, L.; Goodman, L. *J. Chem. Phys.* **1982**, *76*, 4745−4750.
(43) Toro, C.; De Boni, L.; Lin, N.; Santoro, F.; Rizzo, A.; Hernandez, F. E. *Chem.—Eur. J.* **2010**, *16*, 3504−3509.
(44) Tinoco, I. *J. Chem. Phys.* **1975**, *62*, 1006−1009.
(45) Peach, M. J. G.; Benfield, P.; Helgaker, T.; Tozer, D. J. *J. Chem. Phys.* **2008**, *128*, 044118.
(46) Silva, D. L.; Murugan, N. A.; Kongsted, J.; Rinkevicius, Z.; Canuto, S.; Ågren, H. *J. Phys. Chem. B* **2012**, *116*, 8169−8181.
(47) Bonin, K. D.; McIlrath, T. J. *J. Opt. Soc. Am. B* **1984**, *1*, 52−55.
(48) Meath, W. J.; Power, E. A. *J. Phys. B: At., Mol. Opt. Phys.* **1984**, *17*, 763−781.

(49) Guilbault, G. G. *Practical Fluorescence: Theory, Methods, and Techniques*; Marcel Dekker, Inc.: New York, 1973.
(50) Vivas, M. G.; De Boni, L.; Bretonniere, Y.; Andraud, C.; Mendonca, C. R. *Opt. Express* **2012**, *20*, 18600−18608.